Surface Permittivity Estimation of Southern Utopia Planitia by High Frequency RoPeR in Tianwen-1 Mars Exploration

Lilong Zou, *Senior Member, IEEE*, Hai Liu, *Senior Member, IEEE*, Amir M. Alani and Guangyou Fang

***Abstract*—China's Tianwen-1 successfully landed in the southern Utopian Planitia of the Martian surface on 15 May 2021. The Zhurong Rover, equipped with a high frequency full polarimetric Rover Penetrating Radar (RoPeR), travelled 1,921 m to investigate the shallow geological structure and material composition of the Martian weathered layer. In this study, we propose a new processing strategy to estimate surface relative permittivity using the HH and VV reflections of the high frequency RoPeR data. This new strategy is based on the induced field rotation effect, which occurs when orthogonally-polarised electromagnetic waves propagate into an uneven surface with incident angles. 3D time-domain finite-difference simulations were performed using random surfaces with various relative permittivities under the same geometry as the Zhurong Rover. Polarimetric alpha angle versus relative permittivity was then calculated based on the simulation results. At the same time, direct coupling removal, band-pass filtering and channel calibration were performed on the real RoPeR data and clear surface reflections were extracted. The surface reflection amplitudes of the HH and VV were then obtained and the polarimetric alpha angle calculated. Finally, relative permittivity was estimated through the relationship obtained from the simulation results. The average value of the relative permittivity estimated by the proposed approach is 3.292, with a standard deviation of 0.235. This result is consistent with that obtained by orbiting Radar Systems and the low frequency RoPeR system. This study will contribute to the further signal processing and accurate interpretation of real radar data captured by way of RoPeR on Mars.**

***Index Terms*—Mars soil, Rover Penetrating Radar (RoPeR), Tianwen-1, Zhurong Rover, relative permittivity, polarimetric alpha angle**

Manuscript received 22 August 2023; revised 18 December 2023 and 25 January 2024; accepted 14 February 2024. Date of publication xx xx, xxxx; date of current version xx xx, xxxx. This work was supported in part by the National Natural Science Foundation of China under Grant 52179126, and Grant 52379099. *(Corresponding author: Lilong Zou.)*

Lilong Zou is with the School of Computing and Engineering, University of West London, London W5 5RF, U.K. (e-mail: lilong.zou@uwl.ac.uk).

Hai Liu is with the School of Civil Engineering, Guangzhou University, Guangzhou 510006, China (e-mail: hliu@gzhu.edu.cn).

Amir M. Alani is with the Faculty of Engineering, Computing and the Environment, Kingston University, London KT1 2EE, U.K. (e-mail: m.alani@kingston.ac.uk).

Guangyou Fang is with the Aerospace Information Research Institute, Chinese Academy of Sciences, Beijing 100094, China (e-mail: fanggy@aircas.ac.cn).

Digital Object Identifier

I. INTRODUCTION

MARS is one of the four Earth-like planets in our solar system. Because the inclination of its rotation axis and its rotation period are similar to those of Earth, it is the most likely planet for human migration in the future. Mars is also located in the habitable zone of the solar system, and much evidence proves that it once had an environment similar to that of Earth. This, coupled with its abundance of resources, has made Mars a major focus of research for various countries [1]. On 15 May 2021, China's Tianwen-1 (TW-1) lander, carrying the Zhurong Rover, successfully landed in the southern Utopia Planitia in the northern lowlands of Mars (109.925° E, 25.066° N). The Zhurong Rover was successfully deployed onto the planet's surface on 22 May 2021. The rover carries six scientific instruments: the Mars Rover Penetrating Radar (RoPeR), Mars Rover Magnetometer (RoMAG), Mars Climate Station (MCS), Mars Surface Compound Detector (MarSCoDe), Multispectral Camera (MSCam) and Navigation and Topography Cameras (NaTeCam) [2][3]. To date, the Zhurong Rover has travelled 1,921 m along the ancient land-sea interface to the south of the Utopian Plains. Unfortunately, although the Zhurong Rover has exceeded its initial expectations, it can no longer be activated.

The Utopia Plain is a large plain within Utopia. It is recognised as the largest impact basin on Mars and, indeed, in the solar system, having an estimated diameter of 3,300 km. Certain areas of the surface of the Utopia Plain exhibit a fan-shaped topography, with a surface that appears to have been carved from ice cream scoops. The topography is thought to have been formed by the degradation of ice-rich permafrost. The fan-shaped depressions are believed to have been formed by the removal of subsurface material by way of sublimation (possibly interstitial ice), and this process may still be occurring [4]. On 22 November 2016, NASA reported the discovery of a large amount of subsurface ice in the Utopia Plains region. It is estimated that the amount of water detected is equivalent to the volume of Lake Superior [5][6].

Soil structure research and water ice prospecting in the southern Utopia Plain constitute two of the scientific missions of the Zhurong Rover. The interior structure, density and water/ice content of the widespread Martian weathering layer can be revealed with the aid of the RoPeR mounted on the Zhurong Rover. The findings will improve our understanding of climatic history, geological origin, habitability and resource

exploration, and enhance our ability to support human settlement. It will also assist in the selection of sampling sites for the investigation of potential ancient lifeforms that may have existed on Mars [7][8].

Prior to in-situ investigations, the structure of the Martian subsurface was investigated by Shallow Radar (SHARAD) and Mars Advanced Radar for Subsurface and Ionospheric Sounding (MARSIS) orbiting radar systems. The permittivities of strata beneath the polar ice caps, hidden ice deposits across Mars and dry rocky materials such as lava flows and pyroclastic deposits have been estimated based on SHARAD (20 MHz centre frequency) and MARSIS (1.8, 3, 4 and 5 MHz sounding modes) [9]-[12]. Due to the low working frequency and orbit altitude, orbiting radar systems were unable to provide detailed information on the structure of the subsurface. In contrast, RoPeR operates on the surface and can provide higher resolution information for the inspection of the shallow surface. The ground penetrating radar (GPR) operating in Chang'E-3, Chang'E-4 and Chang'E-5 on the lunar surface is effective in revealing the underlying strata to within a few hundred metres, providing information on high-resolution images of underground structures, estimating relative permittivity to further analyse the composition of lunar soil, and so on [13]-[17].

Extensive use of GPR technology has been realized on Earth, including applications in landmine detection, archaeological research, pavement analysis, and civil and environmental engineering [18]-[20]. Using electromagnetic (EM) waves, GPR produces high-resolution subsurface images. The relative permittivity of the material determines the EM propagation speed. Various methods can be employed to measure relative permittivity, such as depth-to-velocity conversion, hyperbolic fitting, common middle points, direct sampling and full-waveform inversion. Due to the special nature of planetary exploration, the hyperbolic method is widely used in the relative permittivity estimation of the rover mounted GPR data. Researchers have utilised this method to calculate relative permittivity for the Martian Rover radar data, including “RIMFAX”, the GPR carried by the Perseverance Rover [21]-[23] and the RoPeR mounted on the Zhurong Rover [24][25].

Based on the ray tracing theory of EM wave propagation into the subsurface during GPR survey, the reflection from a single target at a certain depth appears as a hyperbola shape in the B-scan. By fitting to the hyperbola response, the relative permittivity of the background material can be estimated. Therefore, accurate estimation requires a smooth interface, uniform material and small target size. However, due to target shape, antenna offset, surface topography and non-homogeneous background material, this method typically provides imprecise results [16]. Various methods have been proposed to increase the accuracy of the relative permittivity estimation of rover mounted GPR data. In the Chang'E-4 mission, a spherical target is assumed in the hyperbolic fitting of Lunar Penetrating Radar data, to obtain relative permittivity [26]. In the Chang'E-3 mission, the height of the radar antenna is considered to enhance dielectric constant inversing technique accuracy [27]. Based on this, antenna spacing is considered to further increase estimation accuracy [28]. Further, hyperbolic fitting requires a certain burial depth of the target. Estimated relative permittivity is the value of material around the target. The common approach to estimating surface relative permittivity is to assume that the background material is homogeneous or interpolated from the background material relative permittivity. It is obvious that surface relative permittivity cannot be precisely estimated for planetary exploration in this way. In the Chang'E-5 mission, the first antenna-array GPR has deployed for the investigation of lunar subsurface structures. By considering the antenna configuration and interface reflection point relationship, the velocity spectrum of a subsurface structure can be estimated and thereby predict relative permittivity. The array GPR can provide accurate subsurface relative permittivity but multiple sets of antennas mean an increase in the payload of the spacecraft.

The high frequency RoPeR system mounted on the Zhurong Rover is a full-polarimetric GPR system. It has two orthogonalised oriented transmitting antenna elements and two orthogonalised oriented receiving antenna elements. The transmitting antenna transmits two orthogonalized polarimetric EM waves (H and V) parallel to the surface, and the receiving antenna receives the reflected orthogonalized polarimetric EM waves (H and V), respectively. Therefore, the system can simultaneously acquire HH, HV, VH and VV reflections from the subsurface. According to the classic Fresnel formula, when two orthogonal EM waves occur on an uneven surface at a certain angle, the direction of the EM wave will alter after transmission into subsurface due to different transmission coefficients. This effect – known as induced field rotation (IFR) – interferes with the reflected energy of the different acquisition modes (HH, HV, VH and VV) [29][30]. However, the influence of this effect becomes complex [31], with regard to roughness and near-field inspection.

In this work, we propose a new approach that considers the IFR effects of orthogonal EM waves and surface roughness, and accurately provides the surface relative permittivity of the southern Utopia Plains on Mars. Surface roughness is modelled based on colour images captured by the MSCam on the Zhurong Rover. Then, a 3D finite-difference time-domain (FDTD) simulation is carried out with the high frequency RoPeR geometry to simulate the IFR effects of different relative permittivities. The relationship of polarimetric alpha angle versus relative permittivity is performed for real data estimation. In the meantime, signal processing on the real dataset is performed to obtain clean surface reflections from the southern Utopia Plains. Finally, using the simulated relationship between the polarimetric alpha angle and relative permittivity, the real value is estimated. This study will contribute to further signal processing, accurate interpretation and precise soil structure research of real radar data from the RoPeR on Mars.

This article is organized as follows. Section II describes the Zhurong Rover high frequency RoPeR system and landing

site. The generated rough surface, 3D simulation and relationship between the polarimetric alpha angle and relative permittivity are also described in this section. In Section III, the real data processing procedure, including antenna coupling removal, band-pass filtering, channel calibration and surface relativity permittivity estimation, are presented. Results and discussions are conducted in Section IV and conclusions follow in Section IV.

II. Methodology And Materials

A. Dataset

In this work, we mainly employed high frequency RoPeR and NaTeCam data, recorded by the Zhurong Rover, which are available from China's Lunar and Planetary Data System (CLPDS) (https://moon.bao.ac.cn).

B. High frequency RoPeR and TW-1 landing region

The main scientific objective of the RoPeR is to characterise the thickness and sub-layer distribution of the Martian soil [32]. RoPeR utilises two channels: a high frequency channel that runs between 0.45 and 2.15 GHz and a low frequency channel that runs between 15 and 95 MHz. The high frequency channel has a range resolution of a few centimetres, while the low frequency channel has a range resolution of several metres. The high frequency data of the RoPeR are used in this work. The transmitting and receiving antenna components are installed at the front of the Zhurong Rover, but positioned at different heights, as shown in Fig. 1 (a). The heights of the transmitting and receiving antennas are 0.345 m and 0.306 m, respectively. The offset of the antenna is 0.42 m. In contrast to the Lunar Penetrating Radar of Chang'E-3/4, RoPeR uses a Linear Frequency Modulation (LFM) technique to circumvent the necessity of a high-voltage source [8]. The space sampling interval of high frequency RoPeR data is 0.05 m. Each high frequency RoPeR trace consists of 2,048 data points with a time window of 235 ns.

Two orthogonally oriented Vivaldi antennas are chosen for use with the RoPeR because of their ultra-wideband property and light weight [33]. The transmitting antenna transmits two orthogonal EM waves parallel to the surface, and the receiving antenna receives the reflected orthogonal EM wave, respectively. Therefore, this method can simultaneously acquire HH, HV, VH and VV reflections from the subsurface. Using this combination, it is feasible to obtain rich information of subsurface target reflections. Polarised orientation calibration, signal processing strategies and discrimination between dry and water ice when utilising high frequency full polarimetric RoPeR data have been studied and provide a valuable direction for future research [34][35].

To date, the Zhurong Rover has travelled 1,921 m along the ancient land-sea interface to the south of the Utopian Plains, as shown in Fig. 1 (b). Along its pathway, the Zhurong Rover passed a number of dunes, highly deteriorated craters and tiny pebbles. The region is relatively flat. The Zhurong Rover is designed to select a flat route, to prevent it from rolling over, and the image at Fig. 1 (b) shows no obvious bumps or obstacles present on the surface of the traversed path.

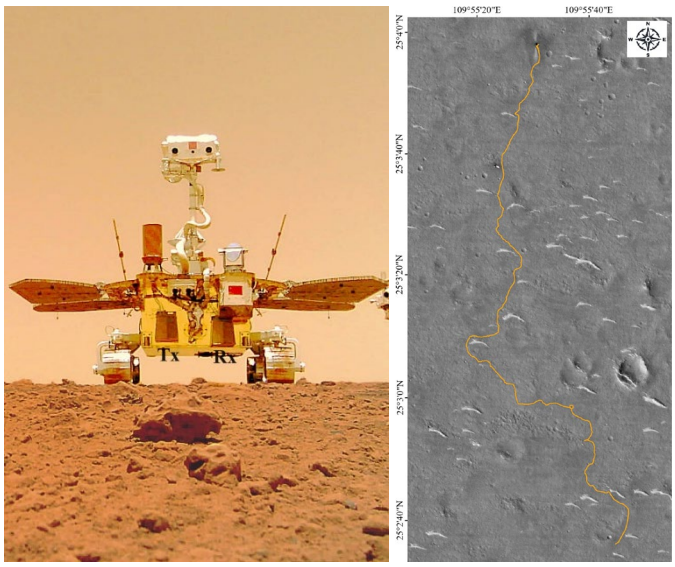

(a) (b)

Fig. 1. (a): Photo of Zhurong Rover; (b) full traversed path.

C. Generating surface roughness

Considering the climatic and environmental conditions on Mars, we use the random Gaussian rough surfaces function to describe the stochastic surface in this paper. Using a random number generator and a Gaussian filter to produce correlation, it is possible to create Gaussian statistics from an uncorrelated distribution of surface points [36]. The surface features a Gaussian height distribution function and Gaussian autocovariance functions (in x and y). Let us assume that there are N_x and N_y points in the x and y directions, respectively, and that the corresponding lengths are denoted as L_x and L_y. Generating the random surface with Gaussian distribution and then scaling using rms height value (h_{rms}), the matrix K is given by:

$$\mathrm{K} = h_{rms} \cdot rand(N_x, N_y). \tag{1}$$

The parameter h_{rms} indicated the root mean square of the height distribution, which is identical to the standard deviation of random surface (expect value is $E[H] = 0$). In order to meet the Nyquist theorem in the spatial domain, the number of points per unit length must be more than twice the inversion of the correlation length:

$$\frac{\max(N_x, N_y)}{\min(L_x, L_y)} > \frac{2}{cl}, \tag{2}$$

where cl indicates the correlation length, which defined the frequency of spatial variations allowed over the surface. Thereafter, the Gaussian filter with low pass frequency is required to produce the spatially correlated surface, and is given by:

$$G = exp\left[-\frac{2(x^2+y^2)}{cl^2}\right]. \tag{3}$$

The final surface Γ is given as a convolution of auxiliary surface K and Gaussian filter G. Therefore, an inverse Fourier transform of a multiplication between K and G is performed in

the spectral domain to produce Γ, and is expressed as:

$$\Gamma = \frac{2L \cdot \mathrm{FFT}^{-1}[\mathrm{FFT(K)} \cdot \mathrm{FFT}(G)]}{\sqrt{\pi} \cdot \max(N_x, N_y) \cdot cl}. \quad (4)$$

Figure 2 presents the NaTeCam photographs captured during the traversing of the Zhurong Rover [37]. The red bar scale in the picture measures 2 cm. As shown in the figure, the size of the soil clods is approximately 1-2 cm. The southern Utopia Planitia is relatively flat, and the Zhurong Rover avoids gravel areas while travelling. Therefore, the roughness of the surface inspected by RoPeR mainly arises from the soil clods. Based on this, rms height $h_{rms} = 0.5\,cm$ and correlation length $cl = 1\,cm$ are given to generate the surface roughness for simulation. The stochastic surface generated by equation (4) is shown in Fig. 3. The random surface has a horizontal correlation length of 1-2 cm and a height of 0.5-1 cm, which match the size of the soil clods, as shown in Fig.2.

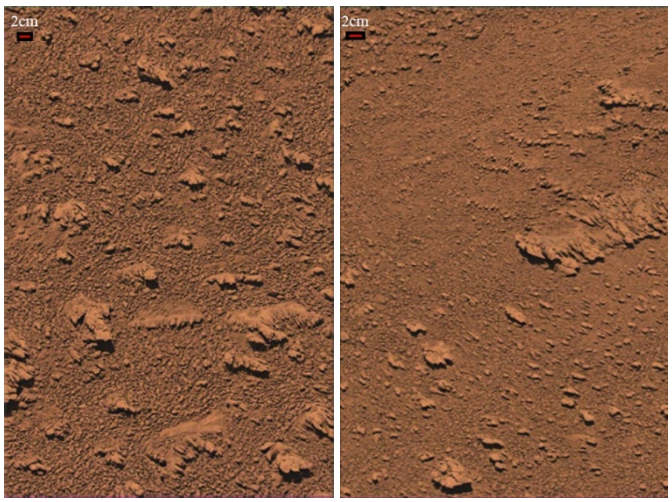

Fig. 2. Colour images captured by MSCam on Zhurong Rover [37].

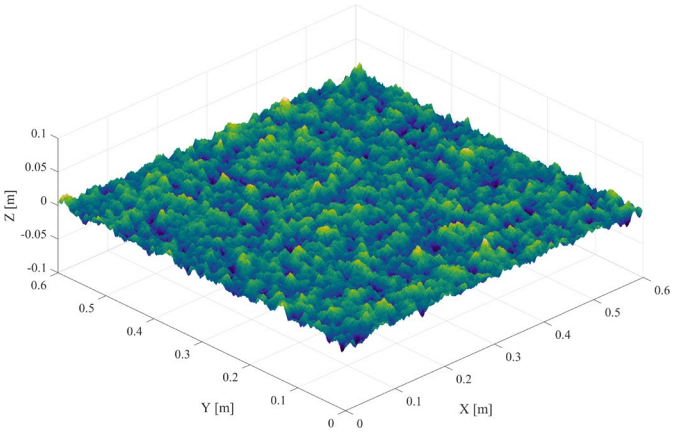

Fig. 3. Generated 3D stochastic surface with 0.5 cm rms height value and 1 cm correlation length for simulation.

D. Simulation and polarimetric alpha angle

In order to investigate the various HH and VV reflections of different relative permittivities under southern Utopia Planitia surface conditions, a 3D FDTD simulation has been adopted using the same transmitter and receiver positions as the RoPeR [38]. The input waveform precisely matches the linearly varying FMCW, with the same start angular frequency, bandwidth and sweep length as the high frequency RoPeR [8].

The stochastic surface model shown in Fig. 3 is used for simulation. The relative permittivity of the surface varies according to the following sequence: 1.001, 1.01, 1.1 to 1.5 with a 0.1 step and 1.5 to 35 with a 0.5 step. Figure 4 shows HH and VV reflections versus the relative permittivity of the stochastic surface. The reflected energy grows as the relative permittivity increases.

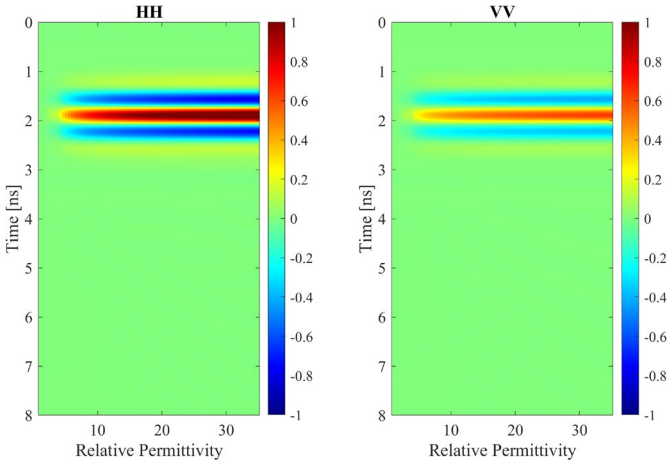

Fig. 4. Simulated HH and VV reflections versus relative permittivity of stochastic surface.

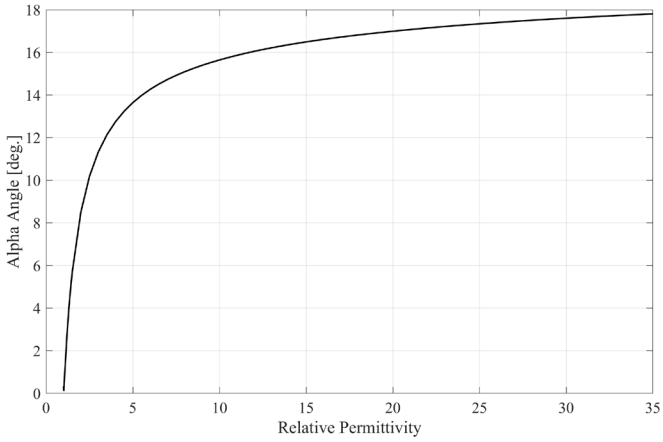

Fig. 5. Simulated relationship of polarimetric alpha angle versus relative permittivity under high frequency RoPeR investigation of Zhurong Rover.

The polarimetric alpha angle is a term commonly used in radar polarimetry, especially in Synthetic Aperture Radar (SAR) polarimetry. The polarimetric alpha angle is used to characterise the scattering mechanism of a given radar target. Specifically, it provides information concerning the type of dominant scattering mechanism exhibited by a particular target [39]-[40]. Based on the Bragg scattering theory, the polarimetric alpha angle is a function of target relative permittivity and the incident angle of the random surface. Therefore, the polarimetric alpha angle is a univariate function

of target relative permittivity with a particular incident angle (e.g., the high frequency RoPeR of the Zhurong Rover). In this paper, we use this relationship to estimate the surface permittivity of the southern Utopia Planitia. The polarimetric alpha angle can be calculated by [41]:

$$\tan\alpha = \frac{S_{VV}-S_{HH}}{S_{VV}+S_{HH}}, \quad (5)$$

where S_{VV} and S_{HH} indicate the scattering coefficients of the VV and HH reflections, respectively. Employing the simulated data shown in Fig. 4, the polarimetric alpha angle versus the relative permittivity of the Zhurong high frequency RoPeR can be calculated and is shown in Fig. 5. The polarimetric alpha angle enlarges as the relative permittivity increases, but it is not a linear relationship. The polarimetric alpha angle changes rapidly when the relative permittivity is small. Although the relative permittivity becomes large, the polarimetric alpha angle changes smoothly.

III. Data Processing and Results

A series of signal processing procedures, including direct coupling (DC) removal, band-pass filtering and channel calibration, were applied to obtain clear, precise surface reflections from the southern Utopia Plains.

A. Antenna coupling removal

Due to the high frequency RoPeR system working frequency bandwidth and the positioning of the transmitter and receiver antennas, the reflection from the surface overlapped with the DC. Removal of the DC is therefore required in order to acquire a clear surface reflection. DC is the wave that directly transmits from the transmitter antenna to the receiver antenna through the air. Therefore, DC is a constant value between different measurement conditions. In this paper, we used the DC as measured in the laboratory of the Chinese Academy of Sciences. The purpose of the indoor test is to confirm the functionality of the device and assess the effectiveness of the rover and radar.

The laboratory indoor measurement was performed using a large metal plate facing towards the RoPeR system. A test pool of 7 m in length, 3 m in breadth and 2.5 m in height makes up the experimental devices [8]. After a metal plate was placed in the pool, the rover was moved from one side to the other to acquire the radar profiles. Figure 6 shows the reflections from the HH and VV channels of the high frequency RoPeR system. The reflections between 10 ns and 20 ns relate to the DC and will be used to subtract the DC from the B-scan acquired on Mars.

B. Band-pass filtering

A band-pass filter is used to remove noise and enhance data quality. Meanwhile, filtering can also be employed to locate hidden patterns and important information in the recorded data. Based on the working frequency bandwidth of high frequency RoPeR, a band-pass filter was employed with cut-off frequencies of 0.75 GHz and 1.85 GHz, as indicated in Fig. 7. The designed filter simultaneously removes the direct current offset and suppresses high frequency noise.

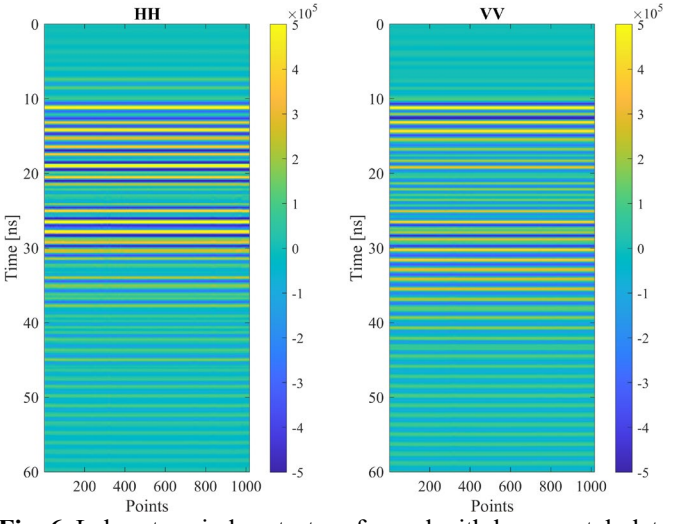

Fig. 6. Laboratory indoor test performed with large metal plate facing towards high frequency RoPeR system.

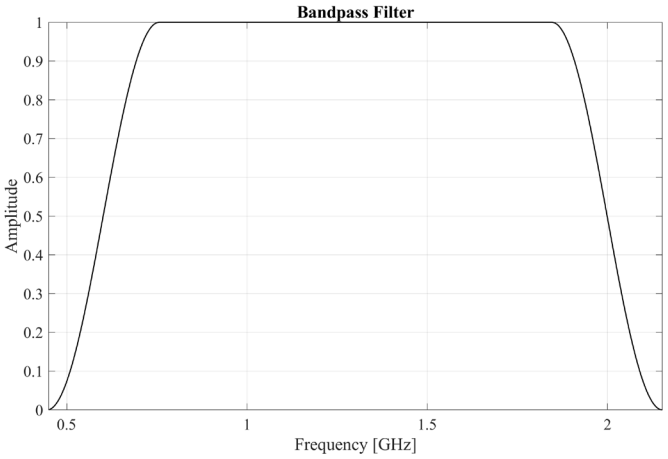

Fig. 7. Designed band-pass filter with cut-off frequencies of 0.75 GHz and 1.85 GHz.

C. Channel calibration

In practice, it is very difficult to design a polarised GPR system with perfect channel balance. To obtain the accurate characteristics of a target using a polarised GPR system, calibration must be performed to remove any system-related contamination. As only the HH and VV channels need to be calibrated, a streamlined approach has been applied in this study. Since the imagery section of the relative permittivity is not studied in this paper, only the amplitude term must be calibrated rather than the phase term. A large metal plate is an ideal target for calibration. The relationship between the HH and VV scattering coefficients of a metal plate is given by:

$$S_{HH} = S_{VV}. \quad (6)$$

Equation (6) indicates that the HH and VV reflections from the metal plate have the same amplitude. The reflections at around 30 ns, shown in Fig. 6, indicate the metal plate, using the high frequency RoPeR system in the laboratory. Looking at the reflection pattern in Fig. 6, it can be observed that the

VV reflection is a little stronger than the HH channel reflection. The entire amplitude of the reflection is calculated through the absolute value of the waveform for calibration. Based on (6), the calibration coefficient of the HH and VV channel of the RoPeR system can be calculated. The calibration coefficient was then used to the real observed data of the Zhurong Rover on Mars. Fig. 8 shows the calibrated B-scan of the HH and VV channels.

D. Surface permittivity estimation

To estimate surface permittivity based on the simulated polarimetric alpha angle described in Section II, the surface reflection coefficients of the HH and VV channels should be calculated. Figure 9 shows the average A-scan of the HH and VV channels, while the B-scan is presented in Fig. 8. The solid red line indicates the HH reflection, while the dashed blue line indicates the VV reflection.

The main lobe of the surface reflection waveform is located at 19 ns. Meanwhile, for the HH reflection, a secondary main lobe appears at 22 ns but does not appear on the VV reflection. We believe this continuously appears reflection in HH channel, but not in VV channel, is not surface reflection. Therefore, this secondary main lobe appears at 22 ns should not be used for surface reflection coefficients calculation. Although regular movement can eliminate this, the surface reflection will then be destroyed. In this study, a window function between 16.4 ns and 21.1 ns is performed to avoid the influence of the secondary main lobe. Therefore, the surface reflection coefficients of the HH and VV channels can be calculated for each acquisition point. In the next step, equation (5) is used to calculate the corresponding polarimetric alpha angle and consequently to estimate the relative surface permittivity.

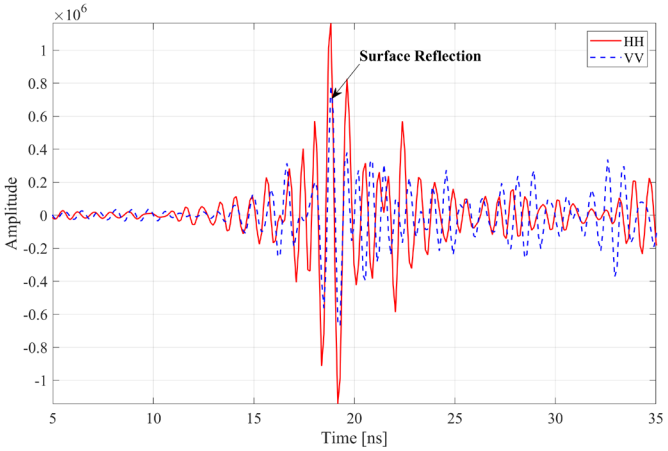

Fig. 9. Averaged surface reflection of HH and VV channels.

IV. Results and Discussions

Upon obtaining the polarimetric alpha angle of each acquisition point, surface relative permittivity along the route taken by the Zhurong Rover can be estimated through the simulation relationship described in Fig. 5. Figure 10 presents

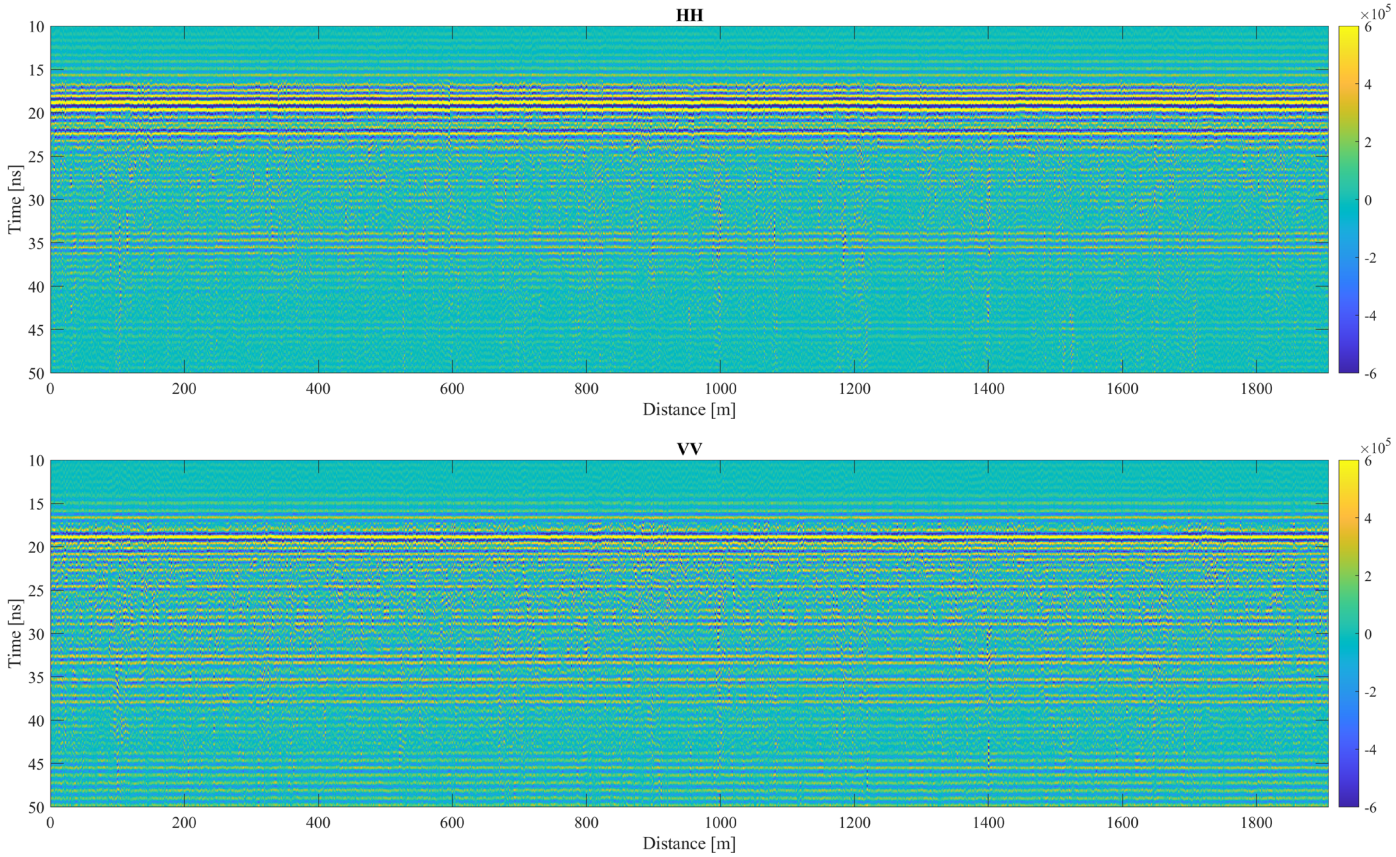

Fig. 8. High frequency RoPeR system B-scan of HH and VV channels after DC removal, band-pass filtering, and channel calibration.

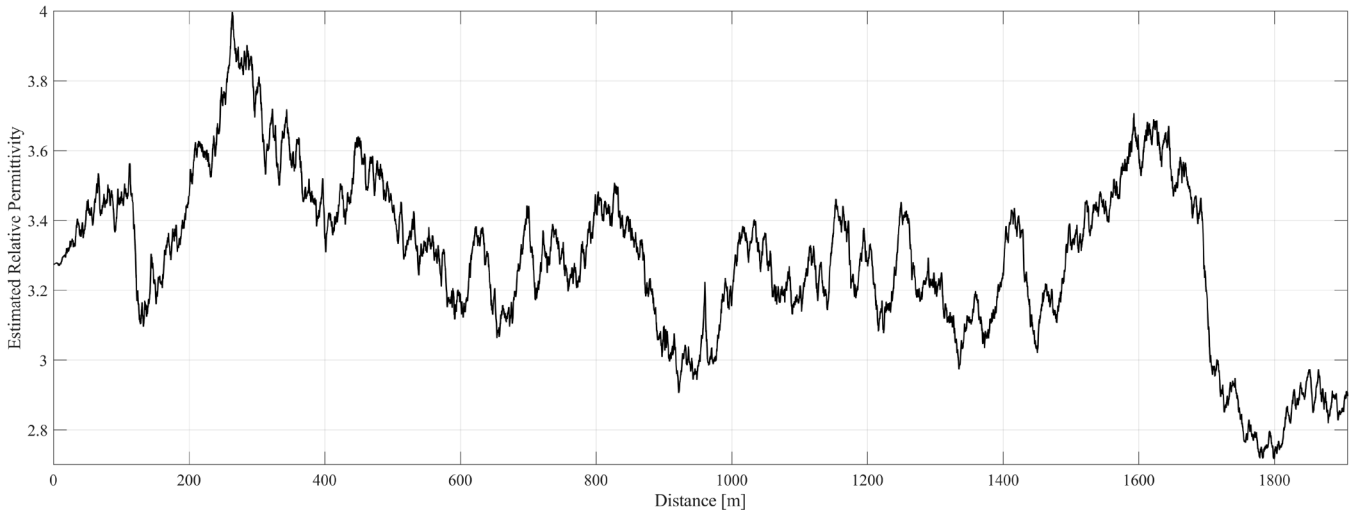

Fig. 10. Estimated surface relative permittivity by the proposed approach.

the estimated relative surface permittivity result of whole Zhurong Rover moving path. The estimated relative permittivity acquired by the Zhurong high frequency RoPeR in the southern Utopia Planitia using the proposed approach has a mean value of 3.292 with and a standard deviation of 0.235. The highest estimated value of 3.997 appears at around 270 m, while the lowest value of 2.717 appears at approximately 1800 m. Castaldo et al. (2017) calculated a relative surface permittivity of about 3 to 4 for the Utopia Planitia region, based on SHARAD data [42]. This result obtained by the proposed approach matches the values measured by MARSIS and SHARAD [9][11]. The estimated relative permittivity is also consistent with the result obtained by the low frequency RoPeR system mounted on the Zhurong Rover [43]. From the result, we can also observe that the relative permittivity suddenly dropped below 3 at a distance of 1,700 m from the landing site of the Zhurong Rover. Based on research using the Lunar Penetrating Radar data of Chang'E-4 [44], this large abnormally relative permittivity is not caused by surface topography, which means that the Zhurong Rover may have entered a new geological zone. This large abnormally relative permittivity will be confirmed with other investigate data in future studies.

V. Conclusion

The high frequency Mars Rover Penetrating Radar (RoPeR) on board the Zhurong Rover is the first and only full polarimetric ground penetrating radar (GPR) to operate on another planet. It provides not only high-resolution subsurface profiles of the southern Utopia area, but also full information on electromagnetic (EM) wave reflections from subsurface targets. In this study, we propose a new processing strategy to estimate surface relative permittivity using HH and VV channels of high frequency RoPeR data. This strategy is based on the induced field rotation effect, which occurs when orthogonal EM waves propagate into an uneven surface with incident angles. A rough surface model was produced by employing colour images captured by the Navigation and Topography Camera (MSCam) located on the Zhurong Rover. Next, 3D Finite-Difference Time-Domain (FDTD) simulations were performed using different relative permittivities and the same geometry as the Zhurong Rover. Finally, the polarimetric alpha angle versus relative permittivity was calculated based on the simulation results.

The proposed method is applied to the high frequency RoPeR data. Before applying the proposed method for relative permittivity estimation, direct coupling removal, band-pass filtering and channel calibration were performed to obtain a clear and precise surface reflection. Then, the reflection coefficients of the HH and VV channels were calculated through the surface reflection and the polarimetric alpha angle was obtained using the reflection coefficients. Finally, relative permittivity was estimated through the relationship obtained from the simulation results. The average value of relative permittivity of the southern Utopia Planitia estimated by the proposed approach is 3.292, with 0.235 standard deviation. The highest estimated value is 3.997, while the lowest value is 2.717. This result is consistent with that of the orbiting Radar Systems-Shallow Radar (SHARAD) and Mars Advanced Radar for Subsurface and Ionospheric Sounding (MARSIS) systems. It also matches the result obtained by the low frequency RoPeR system mounted on the Zhurong Rover. The relative permittivity estimated using the proposed method is the surface permittivity, which differs at deeper depths. Relative permittivity is expected to change with depth due to the density increase. Thus, the proposed approach can only be used to estimate relative permittivity for the first ~0.5 m but can be used to extrapolate deeper depth permittivity combined with other information (e.g., bulk intensity, empirical formula or deeper weathering layers reflection). Therefore, this study will contribute to the further signal processing and accurate interpretation of real RoPeR data from RoPeR on Mars.

References

[1] S. Seager, *Exoplanets*, University of Arizona Press, 2010.
[2] Y. Zou et al., “Scientific objectives and payloads of Tianwen-1, China’s first Mars exploration mission,” *Adv. Space Res.*, vol. 67, no. 2, pp. 812-823, Jan. 2021.

[3] X. Tan, J. Liu, X. Zhang, W. Yan, W. Chen, X. Ren, W. Zuo and C. Li, "Design and validation of the scientific data products for China's Tianwen-1 mission," *Space Sci. Rev.*, vol. 217, pp. 1-22, Aug. 2021.

[4] M. Carr, J. Head, "Geologic history of Mars," *Earth Planet. Sci. Lett.*, vol. 294, no. 3-4, pp. 185-203, Jun. 2010.

[5] G. A. Morgan et al., "Availability of subsurface water-ice resources in the northern mid-latitudes of Mars", *Nature Astron.*, vol. 5, no. 3, pp. 230-236, Mar. 2021.

[6] C. Stuurman et al., "SHARAD detection and characterization of subsurface water ice deposits in Utopia Planitia Mars", *Geophys. Res. Lett.*, vol. 43, no. 18, pp. 9484-9491, Sep. 2016.

[7] W. Wan, C. Wang, C. Li and Y. Wei, "China's first mission to Mars," *Nat. Astron.*, vol. 4, no. 7, pp. 721, Jul. 2020

[8] B. Zhou, S. Shen, W. Lu, Q. Liu, C. Tang, S. Li and G. Fang, "The Mars rover subsurface penetrating radar onboard China's Mars 2020 mission," *Earth Planet. Phys.*, vol. 4, no. 4, pp. 345-354, Jul. 2020.

[9] J. Mouginot, A. Pommerol, P. Beck, W. Kofman and S. M. Clifford, "Dielectric map of the Martian northern Hemisphere and the nature of plain filling materials: Dielectric map of Mars", *Geophys. Res. Lett.*, vol. 39, no. 2, Jan. 2012.

[10] R. Orosei et al., "Radar evidence of subglacial liquid water on Mars", *Science*, vol. 361, no. 6401, pp. 490-493, Aug. 2018.

[11] L. Castaldo, D. Mège, J. Gurgurewicz, R. Orosei and G. Alberti, "Global permittivity mapping of the Martian surface from SHARAD," *Earth Planet. Sci. Lett.*, vol. 462, pp. 55-65, Mar. 2017.

[12] X. Meng, Y. Xu, L. Xiao and Z. Xiao, "Permittivity estimation of subsurface deposits in the Elysium–Utopia region on Mars with MRO shallow radar sounder data," *Astronomical J.*, vol. 159, no. 4, pp. 156, Mar. 2020.

[13] J. Lai, Y. Xu, X. Zhang and Z. Tang, "Structural analysis of lunar subsurface with Chang' E-3 lunar penetrating radar", *Planet. Space Sci.*, vol. 120, pp. 96-102, Jan. 2016.

[14] J. Lai, Y. Xu, X. Zhang, L. Xiao, Q. Yan, X. Meng, B. Zhou, Z. Dong and D. Zhao, "Comparison of dielectric properties and structure of lunar regolith at Chang'e-3 and Chang'e-4 landing sites revealed by ground-penetrating radar", *Geophys. Res. Lett.*, vol. 46, no. 22, pp. 12783-12793, Nov. 2019.

[15] Z. Dong, G. Fang, B. Zhou, D. Zhao, Y. Gao and Y. Ji, "Properties of Lunar Regolith on the Moon's Farside Unveiled by Chang'E-4 Lunar Penetrating Radar", *J. Geophys. Res. Planets*, vol. 126, no. 6, pp. e2020JE006564, Jun. 2021.

[16] H. Zhou, X. Feng, C. Ding, Z. Dong, C. Liu and W. Liang, "Heterogeneous Weathering Process of Lunar Regolith Revealed by Polarimetric Attributes Analysis of Chang'E-4 Lunar Penetrating Radar Data Acquired During the Yutu-2 Turnings", *Geophys. Res. Lett.*, vol. 49, no. 13, pp. e2022GL099207, Jul. 2022.

[17] Y. Su, R. Wang, X. Deng, Z. Zhang, J. Zhou, Z. Xiao, C. Ding, Y. Li, S. Dai, X. Ren and X. Zeng, "Hyperfine structure of regolith unveiled by Chang'E-5 lunar regolith penetrating radar", *IEEE Trans. Geosci. Remote Sens.*, vol. 60, pp. 1-14, Jan. 2022.

[18] L. Zou, F. Tosti and A. M. Alani, "Nondestructive inspection of tree trunks using a dual-polarized ground-penetrating radar system," *IEEE Trans. Geosci. Remote Sens.*, vol. 60, pp. 1-8, Jun. 2022.

[19] L. Zou, L. Yi and M. Sato, "On the use of lateral wave for the interlayer debonding detecting in an asphalt airport pavement using a multistatic GPR system," *IEEE Trans. Geosci. Remote Sens.*, vol. 58, no. 6, pp. 4215-4224, Jan. 2020.

[20] X. Feng, Y. Yu, C. Liu and M. Fehler, "Combination of H-alpha decomposition and migration for enhancing subsurface target classification of GPR," *IEEE Trans. Geosci. Remote Sens.*, vol. 53, no. 9, pp. 4852–4861, Sep. 2015.

[21] S. Eide, T. Casademont, T. Berger, H. Dypvik, E. Shoemaker and S. Hamran, "Radar Attenuation in the Shallow Martian Subsurface: RIMFAX Time-Frequency Analysis and Constant-Q Characterization Over Jezero Crater Floor," *Geophys. Res. Lett.*, vol. 50, no. 7, pp. e2022GL101429, Apr. 2023.

[22] T. Casademont, S. Eide, E. Shoemaker, Y. Liu, D. Nunes, P. Russell, H. Dypvik, H. Amundsen, T. Berger and S. Hamran, "RIMFAX ground penetrating radar reveals dielectric permittivity and rock density of shallow Martian subsurface," *J. Geophys. Res. Planets.*, vol. 128, no. 5, pp. e2022JE007598, May 2023.

[23] N. Oudart, V. Ciarletti, A. Le Gall, Y. Hervé and E. Brighi, "Retrieval of the ground dielectric permittivity by planetary GPR accommodated on a rover: Application to the estimation of the reflectors' depth by the WISDOM/ExoMars radar," *Planet. Space Sci.*, vol. 224, pp.105606, Dec. 2022.

[24] L. Zhang, Y. Xu, R. Liu, R. Chen, R. Bugiolacchi and R. Gao, "The Dielectric Properties of Martian Regolith at the Tianwen-1 Landing Site," *Geophys. Res. Lett.*, vol. 50, no. 13, pp. e2022GL10220, Jul. 2023.

[25] R. Liu, Y. Xu, R. Chen, J. Zhao and X. Xu, "An improved hyperbolic method and its application to property inversion in Martian Tianwen-1 GPR data," *IEEE Trans. Geosci. Remote Sens.*, vol. 61, pp. 1-14, Apr. 2023.

[26] Z. Dong, G. Fang, D. Zhao, B. Zhou, Y. Gao and Y. Ji, "Dielectric properties of lunar subsurface materials," *Geophys. Res. Lett.*, vol. 47, no. 22, pp. e2020GL089264, Nov. 2020.

[27] W. Fa, "Bulk Density of the Lunar Regolith at the Chang'E-3 Landing Site as Estimated From Lunar Penetrating Radar," *Earth Space Sci.* vol. 7, no. 2, pp. e2019EA000801, Feb. 2020.

[28] Y. Feng, S. Chen, X. Tong, C. Wang, P. Li, M. Xi and C. Xiao, "Exploring the Lunar Regolith's Thickness and Dielectric Properties Using Band-Limited Impedance at Chang'E-4 Landing Site," *J. Geophys. Res. Planets.*, vol. 128, no. 3, pp. e2022JE007540, Mar. 2023.

[29] Z. Dong, X. Feng, H. Zhou, C. Liu and M. Sato, "Effects of Induced Field Rotation From Rough Surface on H-Alpha Decomposition of Full-Polarimetric GPR," *IEEE Trans. Geosci. Remote Sens.*, vol. 59, no. 11, pp. 9192-9208, Feb. 2021.

[30] Z. Dong, X. Feng, H. Zhou, C. Liu, Q. Lu and W. Liang, "Assessing the effects of induced field rotation on water ice detection of Tianwen-1 full-polarimetric Mars rover penetrating radar," *IEEE Trans. Geosci. Remote Sens.*, vol. 60, pp. 1-13, Dec. 2021.

[31] K. Chen, L. Tsang, K. Chen, T. H. Liao and J. Lee, "Polarimetric Simulations of SAR at L-Band Over Bare Soil Using Scattering Matrices of Random Rough Surfaces from Numerical Three-Dimensional Solutions of Maxwell Equations," *IEEE Trans. Geosci. Remote Sens*, vol. 52, no. 11, pp. 7048-7058, Apr. 2014.

[32] L. Ding, R. Zhou, T. Yu, H. Gao, H. Yang, J. Li, Y. Yuan, C. Liu, J. Wang, Y. Zhao and Z. Wang, "Surface characteristics of the Zhurong Mars rover traverse at Utopia Planitia," *Nat. Geosci*., vol. 15, no. 3, pp. 171-176, Mar. 2022.

[33] P. J. Gibson, "The Vivaldi aerial", *Proc. 9th Eur. Microw. Conf.*, pp. 101-105, 1979.

[34] H. Zhou, X. Feng, B. Zhou, Z. Dong, G. Fang, Z. Zeng, C. Liu, Y. Li and W. Lu, "Polarized Orientation Calibration and Processing Strategies for Tianwen-1 Full-Polarimetric Mars Rover Penetrating Radar Data," *IEEE Trans. Geosci. Remote Sens.*, vol. 60, pp. 1-14, Nov. 2022.

[35] H. Liu, J. Li, X. Meng, B. Zhou, G. Fang and B. F. Spencer, "Discrimination Between Dry and Water Ices by Full Polarimetric Radar: Implications for China's First Martian Exploration," *IEEE Trans. Geosci. Remote Sens.*, vol. 61, pp. 1-11, Dec. 2022.

[36] N. Garcia and E. Stoll, "Monte Carlo calculation for electromagnetic-wave scattering from random rough surfaces," *Phys. Rev. Lett.*, vol. 52, no. 20, pp. 1798, May 1984.

[37] J. Liu, X. Qin, X. Ren, X. Wang, Y. Sun, X. Zeng, H. Wu, Z. Chen, W. Chen, Y. Chen, C. Wang. Z. Sun, R. Zhang, Z. Ouyang, Z. Guo, J. Head and C. Li, "Martian dunes indicative of wind regime shift in line with end of ice age," *Nature*, vol. 620, no. 7973, pp. 303-309, Aug. 2023.

[38] L. Zhang, Y. Xu, Z. Zeng, J. Li and D. Zhang, "Simulation of Martian Near-Surface Structure and Imaging of Future GPR Data From Mars," *IEEE Trans. Geosci. Remote Sens.*, vol. 60, pp. 1-12, May 2021.

[39] H. Zebker and J. J. Van Zyl, "Imaging radar polarimetry: A review," *Proc. IEEE*, vol. 79, no. 11, pp. 1583-1606, Nov. 1991.

[40] S. R. Cloude and E. Pottier, "A review of target decomposition theorems in radar polarimetry," *IEEE Trans. Geosci. Remote Sens.*, vol. 34, no. 2, pp. 498-518, Mar. 1996.

[41] L. Zou, F. Tosti, L. Lantini and A. M. Alani, "Polarimetric Alpha Angle versus Relative Permittivity with Dual-Polarimetric GPR Experiments," *2021 11th International Workshop on Advanced Ground Penetrating Radar (IWAGPR)*, Valletta, Malta, 2021, pp. 1-3.

[42] L. Castaldo, D. Mège, J. Gurgurewicz, R. Orosei and G. Alberti, "Global permittivity mapping of the Martian surface from SHARAD," *Earth Planet. Sci. Lett.*, vol. 462, pp. 55-65, Mar. 2017.

[43] C. Li, Y. Zheng, X. Wang, J. Zhang, Y. Wang, L. Chen, L. Zhang, P. Zhao, Y. Liu, W. Lv and Y. Liu, "Layered subsurface in Utopia Basin of Mars revealed by Zhurong rover radar," *Nature*, vol. 610, no. 7931, pp. 308-312, Oct. 2022.

[44] C. Ding, Z. Xiao, B. Wu, Z. Li, Y. Su, B. Zhou, K. Liu, J. Cui, "Rock Fragments in Shallow Lunar Regolith: Constraints by the Lunar

Penetrating Radar Onboard the Chang'E-4 Mission," *J. Geophys. Res. Planets.*, vol. 126, no. 9, pp. e2021JE006917, Sep. 2021.

Lilong Zou (Senior Member, IEEE) received the B.S. and M.S. degrees from Jilin University, Changchun, China, in 2009 and 2012, respectively, and the Ph.D. degree from Tohoku University, Sendai, Japan, in 2016.

From 2016 to 2018, he was an Assistant Professor with Tohoku University, Japan. He is currently a Senior Lecturer with the School of Computing and Engineering, University of West London, London, U.K. His research interests include microwave remote sensing, nondestructive testing, and planet exploration radar technology.

Dr. Zou received the Best Award of the Society of Instrument and Control Engineers (SICE) conference, Japan in 2014 and the Best Research Award from Information and Communication Technology for Safe and Secure Life (ICTSSL, Japan) in 2017, and the Best Paper Award of Institute of Electronics, Information and Communication Engineers (IEICE, Japan) in 2021.

Hai Liu (Senior Member, IEEE) received the B.E. and M.E. degrees in civil engineering from Tongji University, Shanghai, China, in 2007 and 2009, respectively, and the Ph.D. degree in environmental studies from Tohoku University, Sendai, Japan, in 2013.

From 2013 to 2014, he was a Research Fellow with the Center for Northeast Asian Studies, Tohoku University. From 2014 to 2017, he was an Assistant Professor with the Institute of Electromagnetics and Acoustics, Xiamen University, Xiamen, China. He is currently a Professor with the School of Civil Engineering, Guangzhou University, Guangzhou, China. His research interests include development of ground penetrating radar systems and algorithms for a wide variety of applications, such as nondestructive testing in civil engineering, environmental monitoring, archeological investigation, and space exploration.

Dr. Liu received the Young Researcher Award at the 14th International Conference on Ground Penetrating Radar in 2012 and the Excellent Paper Award at the IET International Radar Conference in 2013.

Amir M. Alani is currently the Pro-Vice Chancellor (Industry Relation) and the Executive Dean of the Faculty of Engineering, Computing and the Environment at Kingston University, London, UK. He also is the Rochester Bridge Trust Professor of Engineering at the university leading a vibrant team of researchers within the field of non-destructive testing and remote sensing research and applications in the field of civil, structural and environmental engineering and infrastructure. He is an expert in the assessment, repair, and maintenance of civil engineering infrastructure such as bridges, tunnels, and buildings and has extensive work experience with different professional bodies in the fields of engineering and design both in the U.K. and Europe. He has more than 29 years of work experience in the higher education sector and industry in the UK. His research covers a wide spectrum of specialties within the civil and mechanical engineering subject areas. These include, the applications of non-destructive testing methods, environment, concrete technology, geotechnics, soil and foundation engineering, and engineering education. He has authored and co-authored more than 250 journal papers, book chapters, international conference papers, and consulting external reports in these areas.

Guangyou Fang received the B.S. degree in electrical engineering from Hunan University, Changsha,China, in 1984, and the M.S. and Ph.D. degrees in electrical engineering from Xi'an Jiaotong University, Xi'an, China, in 1990 and 1996,respectively.

From 1990 to 1999, he was an Associate Professor, a Professor and Deputy Chief Engineer with the China Research Institute of Radiowave Propagation(CRIRP). From 2000 to 2001, he was a Senior Visiting Scholar with the University of Trieste, and also with the International Center for Science and High Technology—United Nations Industrial Development Organization (ICS-UNIDO), Trieste, Italy. From 2001 to 2003, he was a Special Foreign Research Fellow of the Japan Society for the Promotion of Science (JSPS), working with Tohoku University, Sendai, Japan. Since 2003, he was a Professor, Deputy Director with the Institute of Electronics (IECAS), and the Director of the Key Laboratory of Electromagnetic Radiation and Sensing Technology, Chinese Academy of Sciences (CAS), also a Professor with the University of Chinese Academy of Sciences (UCAS), Beijing, China. Since 2018, he has been a Professor, Vice-President with the Aerospace Information Research Institute (AIRCAS), and also a Professor with UCAS, Beijing. He has authored or coauthored over 400 publications. He is the PI of Chang'E-3/4 Yutu lunar rover penetrating radar, Chang'E-5 Lander MIMO penetrating radar and Tianwen-1 Zhurong Mars rover penetrating radar. His research interests include Ultrawideband Radar, Ground-Penetrating Radar, Lunar/Mars Exploration Radar, Through Wall Radar, Subsurface EM Detection Methods, Terahertz and Computational Electromagnetics.